Mon. Not. R. Astron. Soc. **000**, 000–000 (0000) Printed 18 October 1994

High resolution radio images of the symbiotic star R Aquarii*

S.M. Dougherty[1], M.F. Bode[1], H.M. Lloyd[1], R.J. Davis[2,3] and S.P. Eyres[2]

[1] *Chemical and Physical Sciences, Liverpool John Moores University, Byrom St., Liverpool, L3 3AF*

[2] *University of Manchester Nuffield Radio Astronomy Laboratories, Jodrell Bank, Macclesfield, Cheshire SK11 9DL*

[3] *NRAO, PO Box 0, Socorro, N.M., 87801, USA*

18 October 1994

ABSTRACT

We present MERLIN radio observations of the nearby symbiotic star R Aquarii at 5 and 1.7 GHz with respective nominal resolutions of ~ 0.04 and 0.13 arcseconds, comparable to the resolution of the optical and ultra-violet images obtained with the HST. Comparison with the HST images shows that the radio emission is associated with features observed at optical and UV wavelengths. In particular, this comparison demonstrates that we have resolved the radio emission from the binary system at the core of R Aquarii. Using the Seaquist, Taylor and Button (1984) model for radio emission from symbiotic stars, we derive the mass loss rate of the Mira to be $\sim 10^{-6}$M$_\odot$ yr^{-1}, which is typical for Miras. Observations at two frequencies provides the spectral index distribution. We find that the features C1, C2 and A$'$ have spectral indices commensurate with thermal emission. The nature of the emission on feature A is not clear, though we argue that is also thermal. It is apparent that the fluxes in features C2 and A$'$ have changed between our observations and those of Kafatos et al. (1989). The 5 GHz flux of feature A$'$ has increased by a factor of 17 over a decade. We discuss the evolution of the emitting region, in terms of shock heating by an interaction with an outflow from the central binary, and find that an outflow velocity of at least 300 km s^{-1} is required, consistent with the model of Solf (1992).

Key words:

1 INTRODUCTION

R Aquarii is a D-type symbiotic containing a M7 Mira long period variable (LPV) of 387 day period and a suspected white dwarf companion in a ~ 44 year binary orbit (Willson et al. 1981). The central region of the system is surrounded by a symmetric nebulosity with two main components, first observed by Lampland (1923). The "outer" nebulosity is an oval shaped structure extending ~ 90 arcseconds in an E-W direction about the Mira. The second component is the "inner" nebula that reaches ~ 30 arcseconds to the N and S of the Mira (Solf & Ulrich 1985). In 1977, a bright "jet-like" feature in the inner nebula became apparent at optical wavelengths (Wallerstein & Greenstein 1980; Herbig 1980). Subsequently, the radio counterpart to this feature was detected at 5 GHz (Sopka et al. 1982) and found to extend ~ 10 arcseconds to the NE of the Mira, corresponding to ~ 2000 AU at an adopted distance of 200 pc.

The region within 10 arcseconds of the Mira has now been observed extensively at optical and radio wavelengths at high spatial resolution. Very Large Array (VLA) observations show that the radio emission arises from several discrete regions (Kafatos et al. 1983; Hollis et al. 1985). To the NE of the emission at the position of the Mira, radio emission arises from three discrete knots of emission, known as features A, B, and D, at increasing distance from the Mira. Another discrete knot of emission, feature A$'$, lies to the SW of the Mira where there is also a more extensive region of low surface brightness emission (B$'$) extending ~ 10 arcseconds to the SW from the Mira (Kafatos et al. 1989). The highest resolution radio observations reveal that the radio emission within ~ 1 arcsecond of the Mira arises from two components known as C1 and C2 (Hollis et al. 1986). C1 is approximately coincident with the Mira, and C2 is 0.8 arcseconds to the NE.

The Hubble Space Telescope (HST) has been used to obtain high resolution optical and UV images of R Aquarii (Paresce et al. 1991; Paresce & Hack 1984, hereafter PH). In particular, the optical images show that the resolved central

* Based on observations made with MERLIN, a national facility operated by University of Manchester on behalf of PPARC

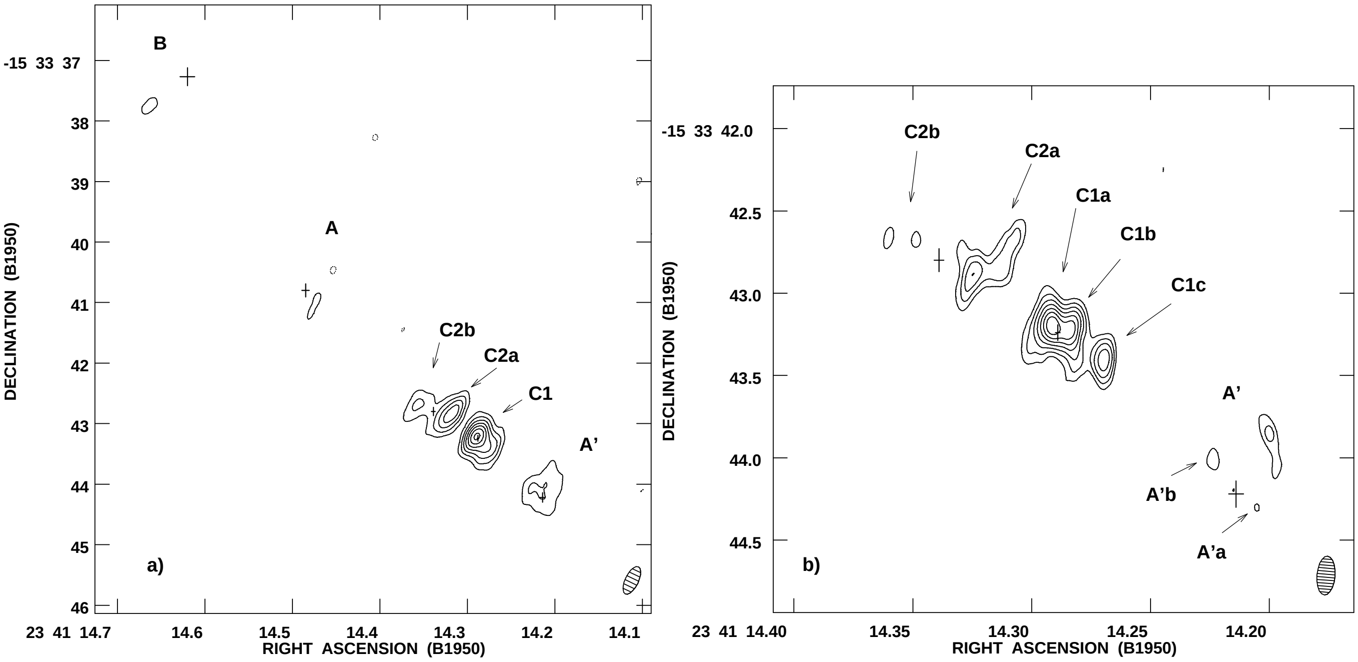

Figure 1. C band MERLIN images of R Aquarii. The visibility data were tapered with a) 1 Mλ and b) 2 Mλ tapers, giving a synthesised beam FWHM of 0.50×0.22 arcseconds and 0.24×0.11 arcseconds respectively, shown in the lower right-hand corner of each image. The 1σ noise and contour levels in a) are 230 μJy and $-3, 3, 5, 7, 9, 11, 13, 15\sigma$, and in b) are 180 μJy and $-3, 3, 4, 5, 6, 7, 8, 9\sigma$. The crosses indicate the estimated positions at epoch 1992.98, equinox B1950, of the previously identified radio emitting features (C1, C2, A, B, A$'$), as deduced from the proper motions of Lehto and Johnson (1992). The 3σ features A$'$a and A$'$b are coincident with the features clearly detected at L band (figure 2).

knots of emission (C1 and C2) consist of several discrete features, one of which PH have identified with the Mira. These features are part of a continuous, well collimated stream of material extending from within $\sim$ 15 AU of the Mira out to $\sim$ 700 AU (3-4 arcseconds) to the NE, close to the position of radio feature A, before breaking up into discrete components. A stream of material is also observed extending to the SW, in a "counter-jet" feature. Several models have been advanced to explain the origin of the emission features in the R Aquarii jet. It is now thought that the discrete features are condensations associated with the expanding "inner" nebula which have been shock excited by a highly collimated, supersonic wind ($\sim 300 - 500$ km s^{-1}) from the binary system (*e.g.* Solf 1992).

In this paper we present radio observations of R Aquarii obtained with the Multi-Element Radio Linked Interferometer Network (MERLIN) (Thomasson, 1986) with a resolution comparable with the resolution using the HST. In this manner we can determine the distribution of the radio emission in the features C1 and C2 and make a direct comparison with features observed with the HST. In addition, we have obtained observations at 1658 MHz to investigate the spectral index distribution at a resolution of $\sim$ 0.5 arcseconds.

2 OBSERVATIONS

Observations at 5 and 1.7 GHz were obtained using the Nuffield Radio Astronomy Laboratory MERLIN interferometer array on the 22 December 1992 (5 GHz), 23 August 1993 and the 31 August 1993 (1.7 GHz). One intermediate frequency was used with a bandwidth of 16 MHz. The longest baseline is 215 km, giving a nominal resolution of 0.04 arcseconds and 0.13 arcseconds at 5 GHz (C band) and 1.7 GHz (L band) respectively. The total integration time on R Aquarii was approximately 300 minutes for each observation, interleaved with frequent observations of the nearby phase calibrator source 2345-167. The absolute flux density scale was established by an observation of 3C286, whose flux density was assumed to be 7.309 Jy and 13.639 Jy at C and L bands respectively. This leads to a flux density for 2345-167 of 2.088 Jy and 2.207 Jy at C and L bands respectively.

The data were initially edited and amplitude calibrated using MERLIN software. Phase calibration and mapping were then carried out using the Astronomical Image Processing (AIPS) software of the National Radio Observatory†. The visibilities for the phase reference source were calibrated using the self-calibration technique. The resulting complex antenna gains were then interpolated to the R Aquarii data.

Images were produced from naturally weighted and tapered visibility data. Tapering essentially weights the visibility data by a factor $w(x) \propto \exp(-(x/x_o)^2)$, where x is the baseline length and x_o is the taper length. This results in a loss of resolution due to an increase in the effective beam. However, both the sensitivity to extended emission and the dynamic range of the images is increased. At L band, we have combined the two sets of observations to reduce the r.m.s. noise in the image by a factor of $\sqrt{2}$. The proper motion of the sources of radio emission is insignificant over the

† The NRAO is operated by Associated Universities, Inc., under contract with the U.S. National Science Foundation.

Table 1. Summary of fluxes and positions of the radio features in R Aquarii

	Feature	Flux[a] (mJy)	Position[b] α (1950)	δ (1950)	Source Dimensions[c] $\theta_{maj} \times \theta_{min}$	PA	
5 GHz	C1a	2.59 ± 0.25	23 41 14.291	-15 33 43.20	0.16×0.09	108	1[d]
	C1b	2.16 ± 0.24	14.284	43.22	0.14×0.12	151	1
	C1c	1.57 ± 0.18	14.270	43.41	$< 0.24 \times 0.11$		1
	C2a	4.10 ± 0.23	14.318	42.84	0.41×0.10	122	2
	C2b	2.22 ± 0.25	14.358	42.70	0.29×0.12	77	2
	A$'$	3.42 ± 0.36	14.214	44.11	0.42×0.31	84	3
1.7 GHz	C1	1.22 ± 0.19	23 41 14.290	-15 33 43.20	$< 0.55 \times 0.38$		4
	C2	3.63 ± 0.32	14.318	42.59	0.69×0.57	77	4
	A	1.31 ± 0.19	14.485	41.04	$< 0.55 \times 0.38$		4
	A$'$a	1.72 ± 0.25	14.210	44.28	0.57×0.35	90	4
	A$'$b	1.27 ± 0.23	14.228	43.85	0.46×0.13	82	4

[a] Fluxes were determined by elliptical gaussian fitting using the AIPS routines JMFIT. For regions that are clearly non-gaussian we used the routine IMSTAT. In each case, a zero level flux was also determined. The integrated flux error for a given figure is the product of the map r.m.s. times the square root of the number of beam areas encompassing the feature.
[b] Positions are given for equinox B1950, epoch 1992.98 (5 GHz) and epoch 1993.66 (1.7 GHz).
[c] Determined from elliptical gaussian fitting. Angular sizes are FWHM and in arcseconds. The position angles are in degrees.
[d] Determined from the a) 2 Mλ, 2) 1 Mλ, 3) 500 kλ tapered C band images and the 4) 800 kλ tapered L band image.

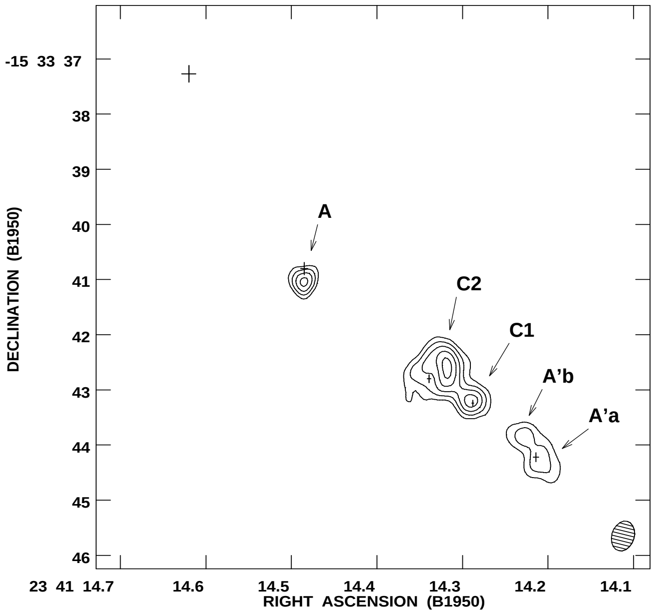

Figure 2. L band MERLIN image of R Aquarii. The data are tapered with a 800 kλ taper, resulting in a beam size of 0.55×0.38 arcseconds. The beam is shown in the lower righthand corner of the image. The 1σ noise level is 190 μJy, and the contour levels are $-3, 3, 4, 5, 6, 7\sigma$. The crosses indicate the estimated positions of the previously identified radio emitting features for epoch 1993.66, equinox B1950.

7 days between the L band observations (Lehto & Johnson 1992, hereafter LJ) and will have no effect on the combined image. The final synthesised images of R Aquarii are shown in figures 1 and 2. The fluxes, positions and angular extent of the features in these images are given in Table 1. The estimated positions of the previously identified radio emission features (C1, C2, A, B, and A$'$) are also shown in the figures, as deduced from the proper motions of LJ.

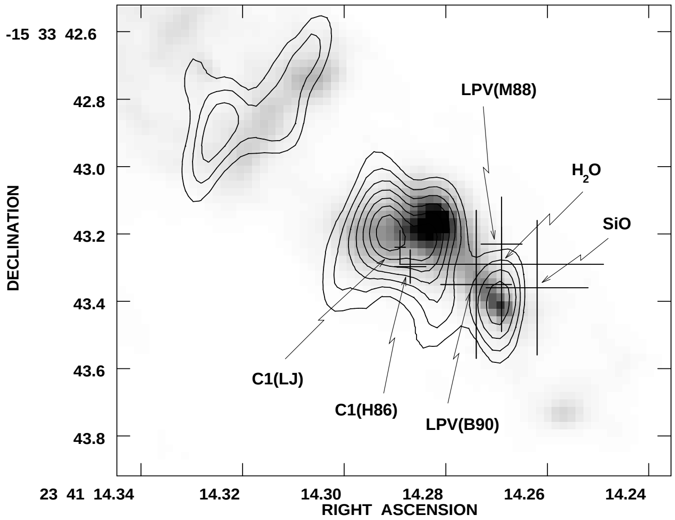

Figure 3. The relative positions of previously identified features and their association to the radio features seen in the observations presented here, namely C1a, C1b, and C1c, and the HST 190 nm image of PH. The radio contours are taken from figure 1b. C1(LJ) is the position of C1 from Lehto & Johnson (1992); C1(H86), from Hollis et al. 1986; LPV(B90), from Baudry et al. 1990; LPV(M88), from Michalitsianos et al. 1988; H_2O, from Ivison et al. 1984; and SiO, from Hollis et al. 1990.

3 IDENTIFICATION OF FEATURES

In addition to the radio emission features that have been previously observed, these high resolution observations reveal for the first time the features that contribute to the radio emission from regions C1 and C2. In this section, we will discuss the identification of these features, with particular reference to features observed using the HST by PH.

In both figures 1a and 1b, the structure in C1 and C2 is clearly evident. The brightest emission at 5 GHz arises from a point we label C1a, which is approximately at the same position as the peak identified in previous radio observations

(Hollis et al. 1986; LJ; see Figure 3). Two additional features close to C1a are also evident, which we label C1b and C1c respectively.

PH have established the position of the Mira in R Aquarii using HST images at 550 nm and 190 nm. At 550 nm the dominant source of emission is the Mira whereas at UV wavelengths the Mira will be much weaker. Comparison of figure 1b with the 190 nm HST image (figure 3) strongly suggests that the radio feature C1c is associated with the Mira, and C1a-C1b with the PH feature N2. In support of C1c being associated with the Mira, its position is consistent with the positions of the Mira derived from ground-based optical observations (Michalitsianos et al. 1988; Baudry et al. 1990) and those of the SiO (Hollis et al. 1990) and H_2O (Ivison et al. 1994) masers assumed to arise in the circumstellar envelope around the Mira (see figure 3). This is confirmed by the χ^2 values for the Mira and maser positions compared to the positions of C1a, C1b and C1c, where the confidence levels associated with the χ^2's are 0.002%, 0.66% and 4.6% respectively. We can therefore rule out component C1a as being associated with the Mira and maser emission. We find that C1c is consistent with the positions for the Mira and maser emission. C1b is marginally consistent with these positions but the relative position of the features in the HST image argues against C1b being the Mira.

For a total system mass of $1.5 M_\odot$ (Burgarella, Vogel & Paresce 1992; hereafter BVP) and an orbital period of 44 years (Willson et al. 1981), the orbit semi-major axis is 2.4×10^{14} cm, corresponding to 0.08 arcseconds at an adopted distance of 200 pc. Hence, the binary system is enclosed within C1c. This is the first time that the radio emission associated with the binary system has been resolved.

At C band, C2 is resolved by MERLIN baselines and is found to consist of two parts: a region elongated in a SE-NW direction 0.54 arcseconds NE of C1a, reminiscent of a Herbig-Haro object and a region 1.12 arcseconds from C1a that is resolved out in the 2 Mλ tapered image. These regions, which we label C2a and C2b respectively, are the radio counterparts to the PH features N3 and the N4-N6 complex. At C band, C2a has a very similar morphology to N3, though at L band the C2 region appears more extended with its peak offset from the peak observed at C band.

The previously observed radio feature A is apparent as a 3σ feature in the MERLIN C band images. It appears as an unresolved region at L band. Recent 5 GHz VLA observations show the flux for feature A to be a few mJy (from examination of figure 1 of LJ). which leads us to conclude that the tenuous detection of A in figure 1 compared to the VLA observations is because the source is largely resolved out on MERLIN baselines.

A number of other previously reported features are not detected in these C band observations. The features D in the NE jet (see LJ) and the extensive feature B$'$ to the SW that was reported by Kafatos et al. (1989) from VLA observations are not observed, even after applying a strong taper to the visibility data. The features B, D and B$'$ are all well resolved on VLA baselines and it is not surprising that their surface brightness is too low to be detected on MERLIN baselines.

The feature A$'$ to the SW of the Mira is clearly resolved, appearing as a cohesive emission feature in figure 1a, yet almost resolved out when a wider taper is applied to the data (figure 1b). At L band it is also resolved, apparently into two

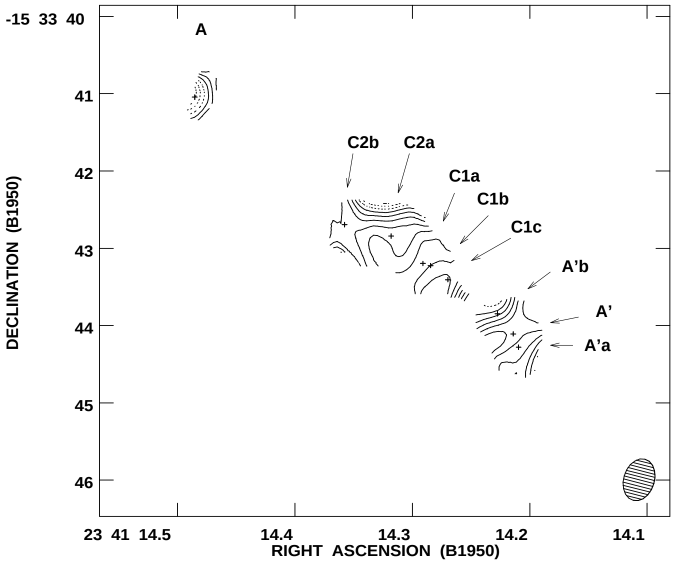

Figure 4. The spectral index distribution of the features within 10 arcseconds of the Mira in R Aquarii. The contour levels are $-0.5, -0.3, -0.1, 0.1, 0.3, 0.5, 0.7, 0.9, 1.1, 1.3, 1.5$. Also marked by crosses are the positions of the features identified in table 1.

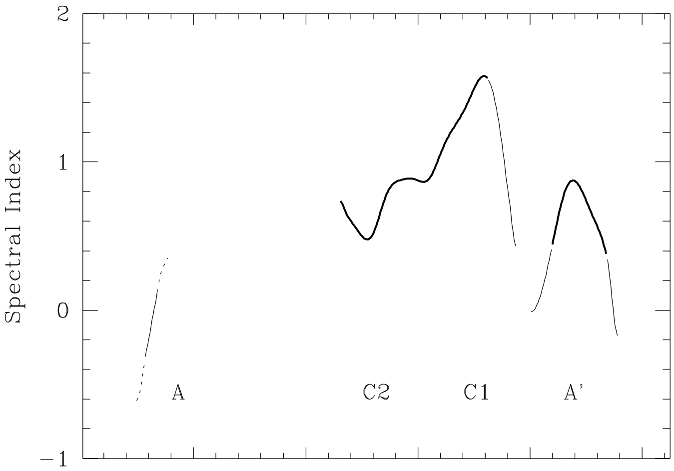

Figure 5. A slice through through the spectral index distribution. The different curves in the slice represent different errors on the spectral index values: $\sigma_\alpha < 0.3$ (heavy solid); $0.3 < \sigma_\alpha < 0.4$ (solid); $0.4 < \sigma_\alpha < 0.5$ (dotted).

features which we label A$'$a and A$'$b. The positions of A$'$a and A$'$b coincide with the positions of emission evident at 5 GHz in figure 1b. These regions appear to be associated with the regions S2 and S3 identified by PH. There is no evidence of a radio counterpart to the PH feature S1.

4 SPECTRAL INDEX DISTRIBUTION

Observations at two frequencies allow us, in principle, to determine the distribution of spectral index in the core region of R Aquarii at the resolution of the 1.7 GHz observations (~ 0.5 arcseconds). At this resolution, the effects of proper motion over the 8 months between the C and L band observations are much smaller than the beam and are effectively smoothed out. We note that in the subsequent analysis it is tacitly assumed that variations in the radio emission from R Aquarii, if any, occur on timescales longer than 8 months.

To calculate the spectral index distribution we first convolved the 5 GHz data with the 1.7 GHz beam. The resulting 5 GHz image was then divided, pixel by pixel, by the 1.7 GHz image to produce the spectral index image shown in figure 4. This gives the spectral index α assuming the convention $S_\nu \propto \nu^\alpha$. Only regions where the error on the spectral index, σ_α, is less than 0.5 are shown in figure 4. We also plot a slice through the distribution that indicates the values of σ_α at different points in the distribution (see figure 5).

The emission in features C1, C2 and A$'$ have positive spectral index values, with a peak value of 1.6 ± 0.3 coinciding with the position of C1c. These values are indicative of partially optically thick thermal free-free emission, an interpretation which is also supported by the brightness temperatures of the features being $\sim 10^3 - 10^4$ K, typical of free-free emitting regions. The overall spectral index of component A$'$ derived from the integral fluxes at 5 GHz and 1.7 GHz is 0.12 ± 0.34, although the spectral index distribution peaks at about 0.9 (see figure 5). This is consistent with the emission being due to largely optically thin thermal bremsstrahlung which is partially optically thick along lines of sight through the centre of the component either due to geometrical effects or central condensation.

Since our observations show that features C1, C2 and A$'$ are emitting free-free radiation, and are all at least partially optically thick at 5 GHz, we can place a lower limit on the r.m.s. electron density in these regions, given by

$$n_e > 2.3 \times 10^8 L^{-1/2}, \quad (1)$$

for a plasma of temperature 10^4 K, where L is the path length through the plasma (in centimetres). Taking the values of angular size given in Table 1 we find that the density is at least 2×10^5 cm^{-3}, similar to values previously derived from UV and radio observations (Hollis et al. 1985; BVP and references therein). This implies that the total mass of these features is $\gtrsim 10^{-6}$ M$_\odot$.

The spectral index value for feature A is more difficult to establish. In figure 5, the error on the spectral index value is such that it could be strongly positive (+1), strongly negative (−1), or both *i.e.* thermal and/or non-thermal in origin. In the case that A is resolved out at 5 GHz, as argued in section 3, we have a lower limit to the total flux at 5 GHz of $\sim$ 1.6 mJy from LJ. This indicates a lower limit to the spectral index of 0.18 ± 0.13, suggesting partially optically thick thermal emission. At 1.7 GHz we can only attribute a lower limit of 4000 K to the brightness temperature, which does not rule out a thermal origin for the emission. It would be beneficial to include observations on shorter baselines to detect any emission that is resolved out at 5 GHz with MERLIN to assist in determining the spectral index of A.

Kafatos et al. (1989) determined the spectral indices for the radio emitting features in R Aquarii from VLA observations at 15 and 5 GHz obtained in the early and mid-1980's. They conclude that C2 and A$'$ contain non-thermal emission, counter to the results presented here. In the data of Kafatos et al., A$'$ is undetected at 15 GHz, with a 3σ upper limit of 0.27 mJy. This is a sufficiently high limit that a positive spectral index, and thus a thermal origin for the emission, cannot be ruled out. In addition, the 1991 observations of Lehto and Johnson appear to show A$'$ at a similar flux level at 8.3 GHz and 5 GHz, indicating a rather flat spectral index at these frequencies. For C2, Kafatos et al. do not give the uncertainty in the measured spectral index, and it is unclear whether the values are significantly different from −0.1, the value expected from optically thin thermal emission. On the other hand, it maybe that the dominant emission mechanism in both C2 and A$'$ has evolved on a time scale of less than a decade.

Indeed, the observations presented in this analysis show that the 5 GHz flux in components C2 and A$'$ are significantly larger in our data than those reported by Kafatos et al., and hence the physical conditions in these components may have changed. In particular, the 5 GHz fluxes have increased by factors of 2.0 ± 0.3 for C2 and 17 ± 3 for A$'$. The 5 GHz flux from component C1 has remained approximately constant, having increased by a factor 1.3 ± 0.4. It is possible that the large flux increase in A$'$ is due to cooling, since at constant pressure, the optically thin free-free flux is proportional to $T^{-1.35}$. In this case, a flux increase by a factor of 17 requires the temperature to be reduced by a factor of 8.2. Assuming that the temperature is currently 10^4 K, and that the 5 GHz flux from component A$'$ is entirely optically thin free-free emission, we obtain a density at the present epoch of 3×10^5 cm^{-3}. Assuming a constant pressure, this implies a cooling time from a temperature of 8.2×10^4 K of the order of tens of days. Thus, changes in flux could occur on very short timescales but are probably dominated by the timescale governing whichever process is responsible for the heating. If this is due to shock heating in a hydrodynamic interaction with an outflow from the central binary, then a ten year timescale for variation would imply a lower limit to the outflow velocity of $\sim$ 300 km s^{-1} (based on the size of A$'$ derived from these observations). Solf (1992) suggests that the "jet" components are shock heated by a collimated wind at a velocity of $300 - 500$ km s^{-1} , so any variation in the conditions in this wind will naturally produce flux variations on timescales of a few to ten years. This timescale for variability could provide an explanation for the conflict between our results and those of Kafatos et al. with regard to the thermal or non-thermal nature of the emission in the various components.

5 MASS LOSS RATE

With the observations presented in this paper, we have resolved the radio emission associated with the binary system for the first time. This allows us to estimate the mass loss rate from the Mira, free of contamination by emission from other nearby emitting features, namely C1a and C1b. The radio emission in C1c is clearly thermal in origin, with a spectral index commensurate with optically thick free-free emission. In this case, and under the assumption of spherical symmetry and an isothermal plasma, we can obtain the mass loss rate using the expression derived by Wright and Barlow (1975). At a constant wind velocity (v) of 30 km s^{-1} and a distance (D) of 200 pc, we obtain a mass loss rate of 1.3×10^{-8} M$_\odot$ yr^{-1} for an electron temperature of 10^4 K. This is slightly lower than previous estimates (*e.g.* Seaquist and Taylor 1990), which is to be expected since earlier estimates have included flux from other emission features in the

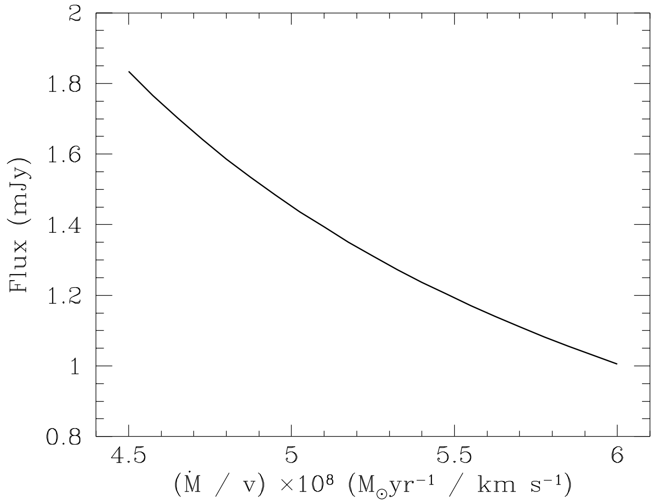

Figure 6. Total flux as a function of $\dot{M}/v$ for the STB model applied to R Aquarii.

core region. More significantly, however, this estimate is two or three orders of magnitude lower than the mass loss rate typically associated with Miras *e.g.* $\sim 10^{-5} - 10^{-6}\,\mathrm{M}_\odot\ \mathrm{yr}^{-1}$ (see Mennessier & Omont 1987 and references therein). The mass loss rate $\dot{M} \propto vD^{\frac{3}{2}}$ and thus an unrealistically high velocity or distance would be required to explain this discrepancy. A more plausible explanation is that the Mira wind is not completely ionised. Certainly, the Wright and Barlow mass loss rate assumes a completely ionised wind and thus represents a lower limit in the case of an incompletely ionised envelope. There is evidence that the Mira wind in R Aquarii may not be completely ionised: the hot component has a weak UV continuum compared to other symbiotic systems (Kenyon 1986), and its radio luminosity is low compared to its infra-red emission (Seaquist, Krogulec & Taylor 1993) compared to other systems. Furthermore, the existence of SiO maser emission is consistent with a small ionised volume.

To allow for the possibility that the Mira wind is not totally ionised, we turn to the model of Seaquist, Taylor and Button (1984, hereafter STB) for the radio emission in symbiotic stars. In this model, free-free emission arises from ionisation of the giant star wind by UV photons from the hot companion star. The size of the ionised region is parameterised by the factor X, which for a pure hydrogen nebula is given by

$$X = \frac{4\pi m_H^2}{\alpha^{(2)}} a L_{ph} \left(\frac{\dot{M}}{v}\right)^2, \qquad (2)$$

where a is the binary separation of the system, L_{ph} is the number of hydrogen ionising photons per second from the hot star, m_H is the mass of a proton, and $\alpha^{(2)}$ is the total recombination coefficient to all but the ground state of hydrogen. Assuming that the hot companion has a radius of 0.1 $\mathrm{R}_\odot$ and an effective temperature 40 000 K (BVP), $L_{ph} = 1.2\times10^{45}\ \mathrm{s}^{-1}$. For a binary separation of 2.4×10^{14} cm, $X = 10^{-16}(\dot{M}/v)^{-2}$.

Adopting the STB model we can estimate the mass loss rate of the Mira in R Aquarii. The size of the emitting region in the STB model is determined from the definition of X (STB, appendix A; Seaquist, Taylor & Button 1987). Assuming the ionised plasma is isothermal with a temperature of 10^4 K and the Mira wind has constant velocity, we have solved the radiative transfer equation for the free-free emitting, ionised region around the hot component. Since the (optically thick) flux is dependent on the solid angle of the emitting region, and hence is sensitive to the density of the wind *i.e.* $\dot{M}/v$ (see equation 2), we have calculated the flux at 5 GHz as a function of $\dot{M}/v$ (Figure 6). The observed 5 GHz flux from the binary system (1.57 ± 0.18 mJy) requires that $\dot{M}/v = 4.8\times10^{-8}$, which implies a mass loss rate from the Mira of $\sim 5 - 15\times10^{-7}\mathrm{M}_\odot\ \mathrm{yr}^{-1}$, similar to that expected from typical Miras, assuming an outflow velocity in the range $10 - 30\ \mathrm{km\ s}^{-1}$. Furthermore, this value of $\dot{M}/v$ gives $X \sim 0.04$. STB have shown that for values of $X < 1/3$ the emitting region is ionisation bounded. This provides further support for an incompletely ionised Mira wind in R Aquarii. A small ionised volume is also consistent with the observed spectral index of 1.6 *i.e.* almost totally optically thick, as expected for an ionisation bounded region. Thus we have demonstrated that the radio flux from C1c is commensurate with that expected from a symbiotic system with a partially ionised Mira wind.

6 SUMMARY

In summary, we have obtained high resolution observations of the radio emission from the symbiotic system R Aquarii, within a few arcseconds of the Mira. We detect features which are clearly associated with features previously observed at optical and UV wavelengths with the HST, including the Mira.

We have derived the spectral index distribution of the features C1, C2 and A′ and found them to be thermal in origin, with no evidence of the non-thermal emission previously identified. We attribute this apparent discrepancy to variations in the flux due to evolution of the emission regions on a timescale of less than a decade. In the case of feature A′, the timescale of variation is consistent with shock heating by an interaction with an outflow of at least 300 km s^{-1},as proposed by Solf (1992). The uncertainties in the values of the spectral index for feature A preclude a simple interpretation. We argue that it is likely to be partially optically thick thermal emission.

The resolution of the radio emission from the binary system has allowed us to obtain an estimate of the mass loss rate from the Mira. The standard Wright and Barlow mass loss rate is $\sim 2 - 3$ orders of magnitude lower than expected for typical Miras. We attribute this to an incompletely ionised Mira wind. Using the Seaquist, Taylor and Button model for radio emission from a symbiotic binary, we estimate the Mira has a mass loss rate $\sim 10^{-6}\mathrm{M}_\odot\ \mathrm{yr}^{-1}$, a typical value for Miras.

Future high resolution radio observations of R Aquarii will provide further insight into the formation of the emitting features in R Aquarii. In particular, a second epoch of MERLIN observations will determine the proper motions of the core features. Combined with high resolution spectroscopy, this will provide the dynamics of the features, which is of particular importance in understanding the association of the radio emitting features to the extensive collimated jet observed with the HST. These observations should be combined with contemporaneous VLA observations so that larger scale (~ 1 arcsecond) emission features will be resolved, an important consideration for investigating the nature of features A, A$'$ and C2.

ACKNOWLEDGEMENTS

We are especially grateful to Drs Paresce and Hack for providing the HST images from their paper prior to publication, and to Dr R.J. Cohen for a number of discussions regarding this work. SMD acknowledges the assistance and enthusiasm of the MERLIN staff during the reduction of the data. This research was supported by grant GR/H 99813 from PPARC.

REFERENCES

Baudry A., Mazurier J.M., Requieme Y., Rousseau J.M. 1990, A&A, 232, 258
Burgarella D., Vogel M., Paresce F. 1992, A&A, 262, 83 (BVP)
Herbig G.H. 1980, IAU Circ., No 3535
Hollis J.M., Kafatos M., Michalitsianos A.G., McAlister H.A. 1985, ApJ, 289, 765
Hollis J.M., Michalitsianos A.G., Kafatos M., Wright M.C.H., Welch W.J. 1986, ApJ, 309, L53
Hollis J.M., Wright M.C.H., Welch W.J., Jewell P.R., Crull H.E., Kafatos M., Michalitsianos A.G. 1990, ApJ, 361, 663
Ivison R.J., Seaquist E.R., Hall P.J. 1994, MNRAS, submitted
Kafatos M., Hollis, J.M., Michalitsianos A.G. 1983, ApJ, 267, L103
Kafatos M., Hollis J.M., Yusef-Zadeh F., Michalitsianos A.G., Elitzur M. 1989, ApJ, 346, 991
Kenyon S.J. 1986, The symbiotic stars, Cambridge University Press, Cambridge.
Lampland C.O. 1923, Publ. Americ. Astron. Soc., 4, 319
Lampland C.O. 1923, Publ. Americ. Astron. Soc., 4, 365
Lehto H.J., Johnson D.R.H. 1992, Nat, 355, 705 (LJ)
Mennessier M.O., Omont A. 1987, (eds) From miras to planetary nebulae: which path for stellar evolution?, Editions Frontières, Gif sur Yvette, France.
Michalitsianos A.G., Oliverson R.J., Hollis J.M., Kafatos M., Crull H.E., Miller R.J. 1988, AJ, 95, 1478
Paresce F. et al. 1991, ApJ, 369 L67
Paresce F., Hack W. 1994, A&A, 287, 154 (PH)
Seaquist E.R., Krogulec M., Taylor A.R. 1993, ApJ, 410, 260
Seaquist E.R., Taylor A.R. 1990, ApJ, 349, 313
Seaquist E.R., Taylor A.R., Button S. 1984, ApJ, 284, 202 (STB)
Seaquist E.R., Taylor A.R., Button S. 1984, ApJ, 317, 555
Solf J. 1992, A&A, 257, 228
Solf J., Ulrich H. 1985, A&A, 148, 274
Sopka R.J., Herbig G.H., Kafatos M., Michalitsianos A.G. 1982, ApJ, 258, L35
Thomasson, P. 1986, QJRAS, 27, 413
Wallerstein G., Greenstein J.L. 1980, PASP, 92, 275
Willson L.A., Garanavich P., Mattei J.A. 1981, IAU Bull. Variable stars, No 1961
Wright A.E., Barlow M.J. 1975, MNRAS, 170, 41

This paper has been produced using the Blackwell Scientific Publications LaTeX style file.